Bioactive SiO_2-K_2O-CaO-P_2O_5 glass-ceramic scaffold prepared using polyurethane foam template

E. R. Essien[1], D. O. Nwude[1], V. E. Okolie[1], L. A. Adams[2]*
[1]*Bells University of Technology, Department of Chemical and Food Sciences, Ota, 112103, Nigeria*
[2]*University of Lagos, Chemistry Department, Akoka, Yaba, 100213, Nigeria*

Abstract

A glass-ceramic in the SiO_2-K_2O-CaO-P_2O_5 quaternary system was prepared by substituting the Na_2O component with K_2O to avoid $Na_2Ca_2Si_3O_9$ formation upon thermal treatment since this phase decreases apatite formation kinetics on glass material. To form the glass-ceramic, a modified sol-gel method involving solution precipitation, followed by reagents encapsulation in citric acid was adopted to enable the use of sodium metasilicate as a cheap substitute for traditional alkoxysilane silica precursors. The foam replication method using polyurethane foam as a sacrificial template was used to obtain the scaffold, which on analysis gave a porosity of 92% and an average pore size of 36±6 μm. *In vitro* bioactivity evaluation in simulated body fluid for a maximum of 14 days indicated the formation of hydroxyapatite on the sample surface. Phase analysis showed that $CaSiO_3$ and K_2CaSiO_4 crystals formed in the sintered sample as the main phases, which exhibited biodegradability in simulated body fluid (SBF). Therefore, economically-derived porous bioactive glass-ceramic scaffolds based on the current method (a simple process) are feasible.
Keywords: bioactive glass-ceramic, carbonated hydroxyapatite, bioactivity, foam replication, polyurethane foam, crystallization, biodegradability.

INTRODUCTION

The specific criteria for an ideal scaffold intended for use in tissue regeneration include [1,2]: a) cell delivery ability; b) outstanding osteoconductivity; c) good biodegradability; d) acceptable mechanical characteristics; e) extremely porous structure; f) irregular shape manufacturing ability; and g) commercialization potential. However, it is challenging to fabricate a material that meets all the foregoing parameters. Bioactive glasses and ceramics have been touted as promising materials for bone tissue regeneration for fulfilling some of these requirements, especially, criteria a to c [3-6]. Bioglass 45S5 (45% SiO_2, 24.5% Na_2O, 24.5% CaO, and 6% P_2O_5 by weight), a degradable silicate glass with a high calcium concentration that can form a link with both soft and hard tissues, was developed by L. Hench in 1969 and is one of the most important biomaterials for bone defect repair [6]. When Bioglass comes into contact with biological fluids, a layer of carbonated hydroxyapatite, similar to the mineral phase of bone, forms on the surface, and silicon and calcium ions are released, which can stimulate the expression of several genes in osteoblastic cells and cause angiogenesis *in vitro* and *in vivo* [7].

To support load-bearing sites before new bone formation, bioactive glasses and ceramics as scaffolds are expected to possess proper mechanical properties. Sodium-containing bioactive glass, including Bioglass 45S5, despite its clinical success [6], is limited by low fracture toughness. Thus, they are usually applied in non-load-bearing regions [8]. To toughen them, they are sintered at high temperatures. A major drawback of this strategy, however, is that it may result in full crystallization, which ultimately reduces the bioactivity of the glass [9, 10]. Various studies [11-14] have shown that the resulting crystal phase contains dense sodium calcium silicate ($Na_2Ca_2Si_3O_9$) which slightly decreases the kinetics of apatite formation on the glass surface. This is due to the slow resorbability of $Na_2Ca_2Si_3O_9$ in body fluid if sintered at high temperatures [15]. During sintering, densification of the sample occurs, pores' volume decreases and there is an overall reduction in the surface area available for reaction. A simple approach that could prevent full crystallization of the glass is to reduce the sintering temperature. However, insufficient densification could produce an extremely fragile scaffold with poorly packed glass particles. To avoid the formation of $Na_2Ca_2Si_3O_9$ during the thermal treatment of sodium-containing bioactive glasses, Cannillo and Sola [16] substituted all the Na_2O in Bioglass 45S5 with K_2O to form glass particles by melting the oxide components at 1450 °C which were then used for coating alumina. Even though they avoided crystallization of the glass, the resulting compact morphology of the coating gave poor apatite nucleation on its surface. Silva et al. [17] substituted Na_2O with K_2O to form potassium-based Bioglass 45S5 and avoided full crystallization when they melted the oxide precursor up to 1350 °C. However, the obtained glass presented irregularly shaped particles and poor pore distribution.

These setbacks could be overcome by combining the relatively low-temperature sol-gel processing technique and the foam replication method to fabricate the scaffold and employing K_2O precursors instead of Na_2O to form a

*eressien@bellsuniversity.edu.ng
https://orcid.org/0000-0003-2379-3640

potassium silicate phase instead $Na_2Ca_2Si_3O_9$ crystalline phase during devitrification. Glasses manufactured by the sol-gel technique possess the advantages of high specific surface area and pore volume as well as nanoporosity which are key to a high rate of hydroxyapatite formation [18]. During sol-gel processing, the condensation, gelation, and drying stages generate fine colloidal particles in the nanometer size dimension and porous morphology with a large surface area. The replication method gives porous scaffolds that can mimic spongy bone [10] and fulfill criteria e to g highlighted above. Despite these benefits, the replication process has never before been employed to prepare SiO_2-K_2O-CaO-P_2O_5 bioactive glass-ceramic scaffolds; instead, the SiO_2-Na_2O-CaO-P_2O_5 system is common. Glasses in the SiO_2-Na_2O-CaO-P_2O_5 system possess the advantage of forming the $Na_2CaSi_3O_9$ crystalline phase and its attendant ability to improve the mechanical property of resulting the scaffold. To substitute K_2O for Na_2O, the melting method was used [16, 17, 19], apparently to achieve a good degree of crystallization and consequently, appreciable mechanical properties. This study, therefore, aimed to synthesize a bioactive glass-ceramic scaffold in the system SiO_2-K_2O-CaO-P_2O_5 through a foam replication technique and a modified sol-gel method by solution precipitation and to assess its bioactivity.

MATERIALS AND METHODS

Materials: to prepare the bioactive glass-ceramic scaffold, the following materials were used: sodium metasilicate ($Na_2SiO_3.9H_2O$, Loba Chemie), calcium nitrate tetrahydrate [$Ca(NO_3)_2.4H_2O$, Loba Chemie], dipotassium hydrogen phosphate trihydrate ($K_2HPO_4.3H_2O$, Sigma-Aldrich), citric acid ($C_6H_8O_7$, Sigma-Aldrich), polyvinyl alcohol (PVA, Sigma-Aldrich) and polyurethane (PU) foam of 15 mm thickness cut into 7.5x7.5x15 mm dimension.

Bioactive glass-ceramic preparation: a bioactive glass (composition by wt%: $35SiO_2$-$35CaO$-$20K_2O$-$10P_2O_5$) was prepared by a modified sol-gel technique involving solution precipitation and precursor encapsulation. In summary, the $Na_2SiO_3.9H_2O$ was dissolved in deionized water and added gradually to $Ca(NO_3)_2.4H_2O$ solution in a conical flask under constant stirring using a magnetic stirrer. The reaction was allowed to continue for 1 h after which the gel formed was poured into a 500 mL beaker and washed with deionized water by swirling the beaker gently to extract the soluble $NaNO_3$ by-product (Eq. A). Thereafter, the supernatant was discarded by decantation. This procedure was repeated thrice and the obtained gel containing $CaSiO_3$ was dried at 120 °C for 72 h.

$$Na_2SiO_3.9H_2O + Ca(NO_3)_2.4H_2O \rightarrow CaSiO_3 + 2NaNO_3 + 13H_2O \quad (A)$$

The as-prepared $CaSiO_3$ powder was added to a solution of 35 wt% citric acid (the encapsulating agent) with constant stirring with a magnetic stirrer unit maintained at 120 °C [14] until it dissolved. After dissolving the $CaSiO_3$,

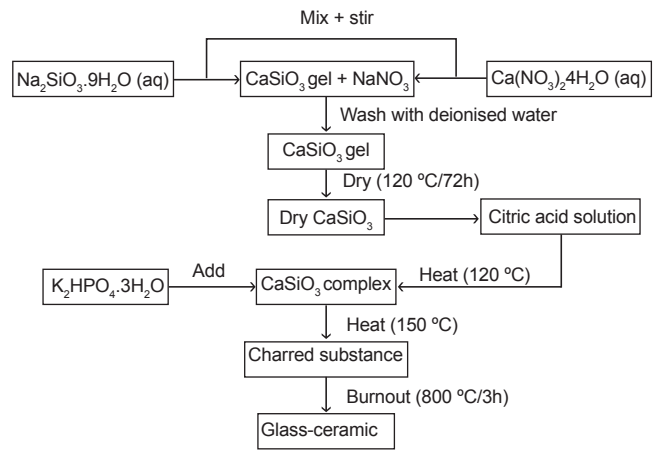

Figure 1: Flowchart summarizing the bioactive glass-ceramic preparation process using a modified sol-gel method.

$K_2HPO_4.3H_2O$ was added and the temperature was adjusted to 150 °C while the stirring was maintained until the mixture was completely burnt. Just before the mixture transformed into a solid mass, the magnetic stirrer bar was withdrawn and the material, thereafter allowed to burn. After cooling to room temperature, the mixture containing the glass was transferred to a furnace for complete burnout at 800 °C for 3 h to destroy the PU template. Part of the resulting monolith was ground into powder for use in preparing the green body. The remainder was labeled BG. The process for obtaining the glass is illustrated in the flowchart presented in Fig. 1.

Preparation of scaffold: the procedure involved the initial preparation of a green body of ceramic foam. Accordingly, a slurry was prepared by adding the bioactive glass-ceramic powder to a 100 mL 0.01 mol/L polyvinyl alcohol (PVA) solution at a 2:3 weight ratio of the bioactive glass-ceramic to PVA solution [10] under vigorous stirring with the aid of a magnetic stirrer for 1 h. Following this, polyurethane foam (dimensions 7.5x7.5x15 mm) was dipped into the slurry and allowed to remain for 15 min. Afterward, the green body was obtained by removing the foam and squeezing out excess slurry. The material was then kept on a smooth surface and allowed to dry ambiently. Thermal treatment to burn out the PU was performed at 400 °C for 2 h, while sintering was carried out at 800 °C for 6 h. The heating rate was 10 °C/min. The bioactive glass-ceramic prepared by using the PU foam as the template was code-named BG_F while that formed without the use of the template was called BG.

The density of the scaffold, ϱ_c, was estimated based on the mass and volume of the sintered bodies. The porosity (P) was determined from [10]:

$$P = \left(1 - \frac{\rho_c}{\rho_s}\right).100 \quad (B)$$

where ϱ_s is the density of 45S5 Bioglass and equals 2.7 g/cm^3 [10]. The pore sizes of the scaffolds were measured on their respective SEM micrographs using the ImageJ software. To assess the microstructure of the samples, a scanning electron microscope (SEM, ProX 800-07334, Phenom-

World, Netherlands) was used. The elemental composition of the sample was determined in an energy-dispersive X-ray (EDX) analyzer unit attached to the SEM machine. The operating voltage was 15 kV, while carbon adhesives were used to attach the samples to a sample holder to allow for their visual observation and the samples were sputter-coated with gold. Diffraction patterns of the samples were obtained from an X-ray diffractometer (XRD, D/Max-IIIC, Rigaku, Japan) to enable phase identification in the samples. The machine was operated using a CuKα radiation source with a wavelength of 0.154060 nm at 40 kV and 40 mA in the 2θ range from 10° to 75°. The strongest diffraction peak in each diffractogram was used to calculate the crystallite size (ζ) of the major phase in the samples, according to the Scherrer equation [18]:

$$\zeta = k.\lambda/(\beta.\cos\theta) \qquad (C)$$

where k is the Scherrer constant (equal to 0.89), λ is the wavelength of the CuKα X-ray (0.15406 nm), and β is the full width at half maximum (FWHM) of the highest diffraction peak. The chemical characteristics of the bonds in the network structure of the bioactive glass-ceramic samples before and after incubation study in simulated body fluid (SBF) to verify the formation of hydroxyapatite (HA) on the surface of the samples was performed using Fourier transform infrared spectroscopy (FTIR, Cary 630, Agilent Technol., USA) in the wavenumber range from 4000 to 650 cm^{-1}.

Determination of bioactivity in simulated body fluid (SBF): to study the ability of the samples to induce apatite formation on their surface, they were immersed in SBF (pH 7.4) at 36.5 °C by following a well-established *in vitro* procedure [20]. The following analytical grade reagents were used to prepare the SBF: NaCl, $NaHCO_3$, KCl, $K_2HPO_4.3H_2O$, $MgCl_2.6H_2O$, $CaCl_2$, tris(hydroxymethyl) aminomethane [Tris-buffer $(CH_2OH)_3CNH_2$, Sigma-Aldrich, USA). During the experiment, the samples were placed in clean plastic containers in the SBF (1 g of sample per 100 mL) and kept in an incubator for a duration of 7 to 14 days. At the end of each immersion period, the samples were removed from the solution, rinsed in sufficient amounts of deionized water by gently swirling the contents, and then placed in a desiccator to dry.

RESULTS AND DISCUSSION

Scaffold microstructure and elemental composition: the morphological architecture of the samples is presented in Fig. 2. The sample prepared without using the PU foam template (BG, Fig. 2a) showed glass particles well-distributed on the bioactive glass-ceramic to present a near-homogeneous

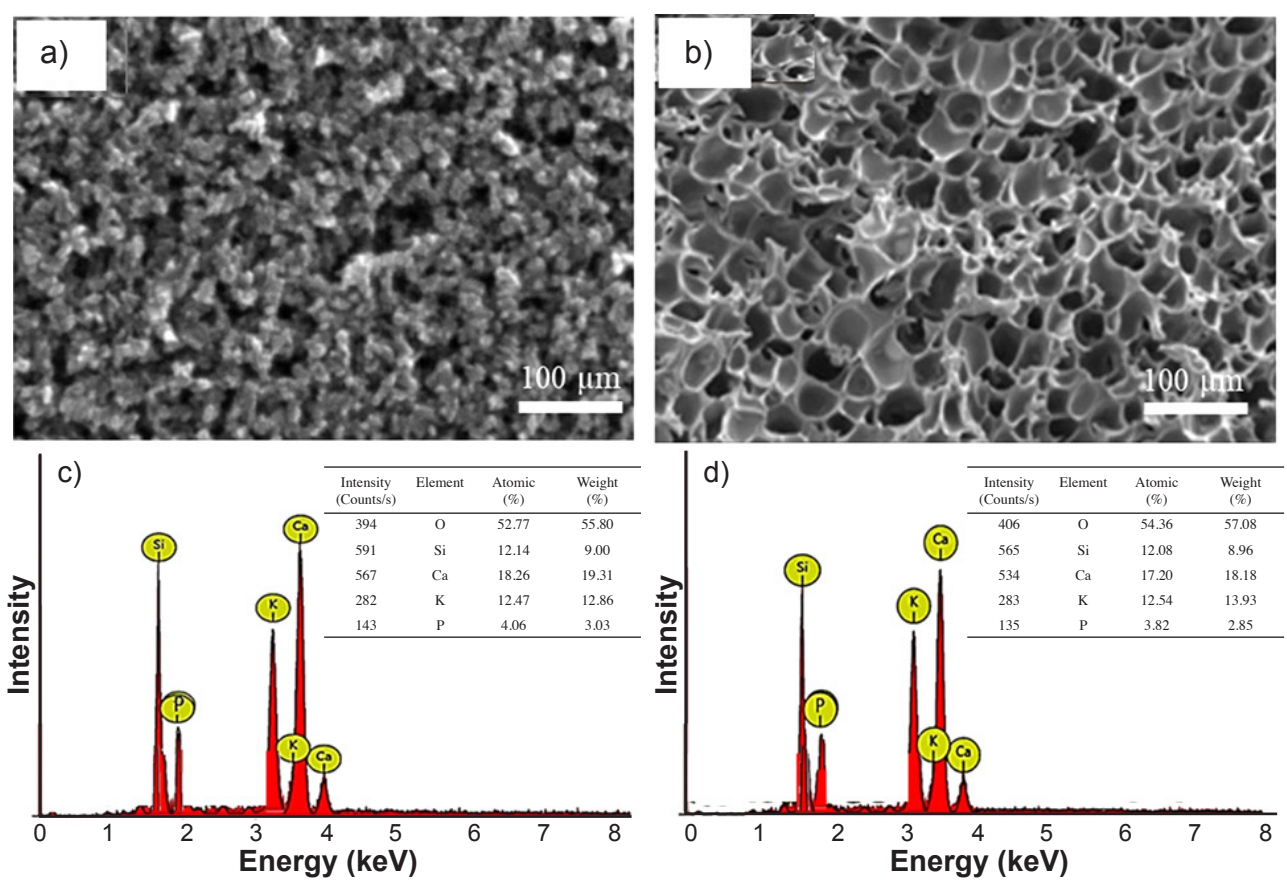

Intensity (Counts/s)	Element	Atomic (%)	Weight (%)
394	O	52.77	55.80
591	Si	12.14	9.00
567	Ca	18.26	19.31
282	K	12.47	12.86
143	P	4.06	3.03

Intensity (Counts/s)	Element	Atomic (%)	Weight (%)
406	O	54.36	57.08
565	Si	12.08	8.96
534	Ca	17.20	18.18
283	K	12.54	13.93
135	P	3.82	2.85

Figure 2: SEM micrographs showing well-distributed particles and pores (a,b) and EDX spectra (c,d) of the glass-ceramic samples sintered at 800 °C for 3 h: a,c) BG; and b,d) BG_F.

surface with a good surface area appearance. However, some of the particles formed clusters and agglomerates, thus giving rise to a few irregularly shaped pore spaces on the surface of the bioactive glass-ceramic. In contrast, a different morphological characteristic was observed in the sample prepared by the replication method using PU foam (BG_F, Fig. 2b). The surface was dominated by a well-defined porous architecture; most of the pores were open and distributed homogeneously over the material surface to present significant microporosity.

The polymer foam template (PU) possessed the desired pore structure and thus served as the sacrificial template during the ceramic coating. Therefore, the final material acquired the microstructure of the sacrificial foam template and hence resulted in a well-ordered glass-ceramic microstructure. BG gave a porosity value of 66% whereas for BG_F the porosity was 92% with pore sizes of 26±5 μm and 36±6 μm, respectively. Sufficient porosity of appropriate size and interconnections between the pores create an environment that promotes cell infiltration, migration, vascularization, nutrition, oxygen flow, and waste elimination while enduring external loading pressures [21]. The capacity of cells to penetrate, proliferate, and differentiate, as well as the pace of scaffold degradation, is greatly influenced by the pore distribution and shape of the scaffold [22]. A minimum of 100 μm has been proposed as the threshold to adequately achieve these functions [14]. Even though the pore size of the scaffold synthesized in this study did not achieve this cut-off value, the high porosity of 92% obtained could enable enhanced cellular activity, according to Loh and Choong [23]. The application of the PU foam increased the pore size of the bioactive glass-ceramic scaffold from 26±5 μm (in BG) to 36±6 μm (in BG_F) by acting as a template. After the burnout, the scaffold mimicked the pore structure of the PU foam. This pore size (36±6 μm), which was in the sub-macropore category, should provide adequate surface area optimum for protein adhesion and cell attachment on the scaffold [24] and even promote ion exchange between the scaffold and the surrounding biological fluid [25].

The elemental composition of BG and BG_F are shown in Figs. 2c and 2d, respectively. As observed, the concentrations of Si, Ca, K, and P present in the glass-ceramic, as designed in both samples, were in agreement with the EDX results. The $CaSiO_3$ formed initially (Eq. A) served as the precursor for CaO and SiO_2 at a 1:1 ratio in the samples upon devitrification at 800 °C/3 h. Also, $K_2HPO_4.3H_2O$ was able to transform into K_2O and P_2O_5 under the same devitrifying condition as depicted in Eq. D. This indicated that the amounts of the starting oxide precursors used as well as the reactions that afforded them were accurate. The absence of a Na peak in the spectrum signified the complete removal of the $NaNO_3$ side product (Eq. A) during the deionized water-washing stage.

$$2K_2HPO_4.3H_2O \xrightarrow{800\ ^\circ C/3h} 2K_2O + P_2O_5 + 4H_2O \qquad (D)$$

Phase formation in samples: the X-ray diffractograms of BG and BG_F (Fig. 3) presented three crystalline phases: wollastonite ($CaSiO_3$), calcite ($CaCO_3$), and potassium calcium silicate (K_2CaSiO_4). The wollastonite peaks matched the standard PDF (JCPDS 00-043-1460) when indexed in angular positions and reflection indices [18]. The K_2CaSiO_4 peaks matched the JCPDS file 19-943 in angular position and intensity, whereas $CaCO_3$ was indexed using the JCPDS file 02-0623. The crystallite size obtained by applying Eq. C was 46 nm. K_2CaSiO_4 crystalline phase has been previously formed and identified in a K_2O-CaO-P_2O_5-SiO_2 system bioactive glass-ceramic [17]. It is interesting to observe the absence of the $Na_2Ca_2Si_3O_9$ phase in the diffractograms of the samples, thus validating the approach adopted in this study. K_2CaSiO_4 should enhance the mechanical property of the scaffold while exhibiting appreciable biodegradability kinetics compared with $Na_2Ca_2Si_3O_9$. The mechanical property and biodegradability of a scaffold should show congruence if it is to be applied at a load-bearing site [10]. The effect of the PU foam template was once again evident as observed in the diffraction patterns of the two samples. The phases formed were similar to those of BG and had an average crystallite size of 33 nm, although they were lower in intensities (Fig. 3b), and appeared to be partially

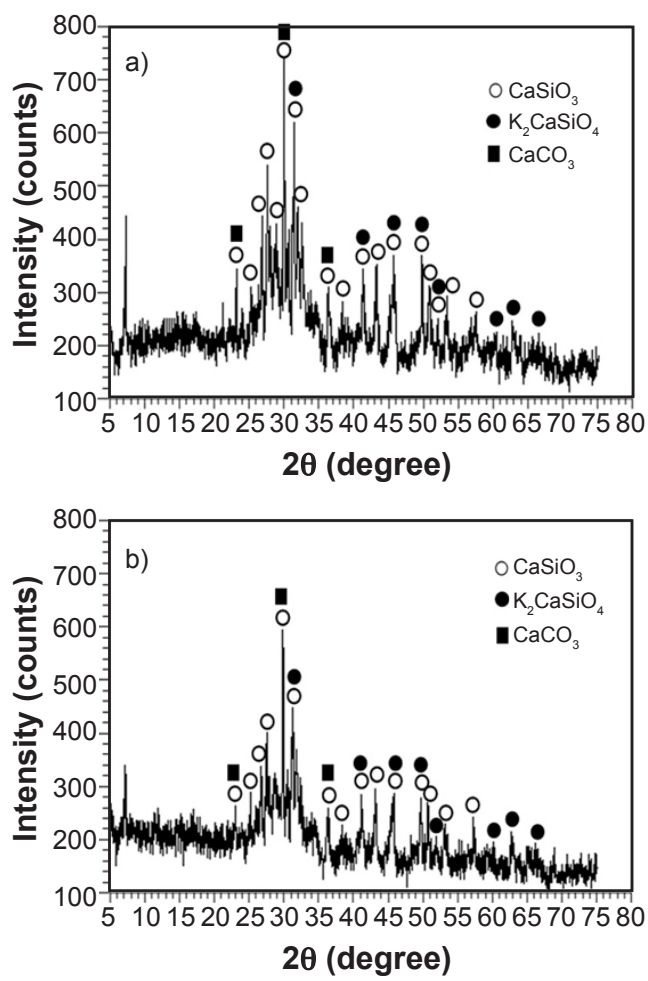

Figure 3: XRD patterns of the samples sintered at 800 °C for 3 h showing the presence of crystalline phases: a) BG; and b) BG_F.

crystallized. This may be attributed to differences in porosity, pore and crystallite sizes of the two samples, which led to the better ordering of atoms in the sample during the thermal treatment. This is an encouraging result, given that crystallization is thought to decrease the bioactivity of a glass or glass-ceramic [9], the higher degree of porosity and, consequently, lower crystallinity are properties desirable for achieving higher bioactivity in implant materials [26].

Assessment of bonds: major peaks in the FTIR spectra, depicted in Fig. 4, were used to confirm the composition of the network structure formed in the glass-ceramic samples. In BG (Fig. 4a), a diagnostic peak for SiO_2 was observed at 1068 cm^{-1} corresponding to siloxane (Si-O-Si) asymmetric stretching vibration [27]. Further vibrational modes of SiO_2 were observed at around 902, 715, and 702 cm^{-1}. The sharp peak around 902 cm^{-1} was attributed to the symmetric stretching of $Si\text{-}O^-$ in SiO_4^{4-} tetrahedron containing two nonbonding oxygen per tetrahedron (Si-O-2NBO) [28], resulting from the presence of K^+ and Ca^{2+} network modifying cations. The formation of two different tetrahedra was confirmed by the small doublet at 715 and 712 cm^{-1}, which were the torsional vibrational modes of Si-O in SiO_4^{4-} [29] due to the presence of K^+ and Ca^{2+} ions. Diagnostic peaks due to the presence of P_2O_5 were indicated by the PO_4^{3-} asymmetric stretching vibration located at 1006 cm^{-1} and the symmetric stretching vibrational mode at 932 cm^{-1} [30]. The bands at around 3450 and 1646 cm^{-1} were ascribed to O-H stretching and angular vibrations, respectively, of water molecules, an indication of the presence of surface water in the samples. The appearance of the prominent CO_3^{2-} peaks near 1476 and 1406 cm^{-1} in the spectrum signified CO_2 adsorption by the material during the preparation stage due to the presence of labile ions (K^+ and Ca^{2+}) in the composition [31]. The presence of these peaks confirmed the calcite peaks earlier observed in the X-ray diffractograms in Fig. 3. The FTIR spectrum of BG_F as shown in Fig. 4b indicated similar vibrational modes to BG, but with minor shifts in the O-H stretching and angular vibrations (3250 and 1648 cm^{-1}) as well as the PO_4^{3-} asymmetric stretching vibration (1002 cm^{-1}) to lower frequencies. This appears to be linked with the lower water content in BG_F caused by PU burnout. Also worthy of note is that no carbonaceous bonds associated with the PU foam template were found in the spectrum of BG_F which affirmed the high purity of the scaffold and the efficiency of the sintering procedure.

Bioactivity evaluation in SBF: bioactivity is usually assessed based on a material undergoing specific surface reactions in the presence of physiological fluids to form hydroxyapatite (HA) on the material surface. The scaffolds were immersed in SBF for a duration of 7 and 14 days after which they were investigated for the presence of HA using SEM, EDX, XRD, and FTIR spectroscopy. The microstructural evolution of the samples after the incubation experiment in SBF is presented in the SEM micrographs in Fig. 5. Colonies containing HA granules formed clusters on the surface of the glass-ceramic as observed in the SEM image of BG after soaking in SBF for 7 days (Fig. 5a),

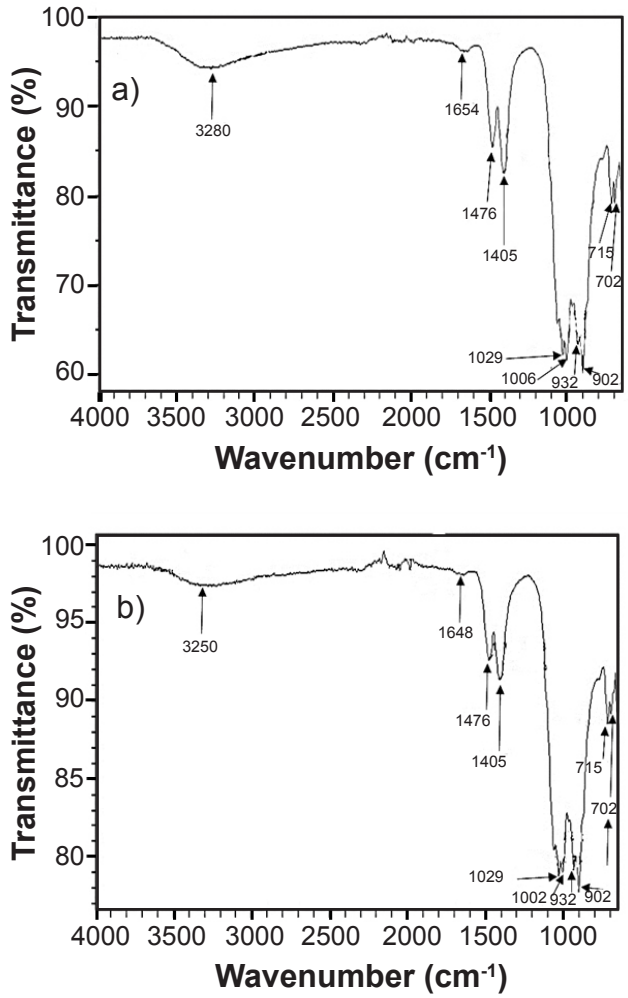

Figure 4: FTIR spectra showing vibrational modes of BG (a) and BG_F (b) samples after sintering at 800 °C for 3 h.

but some portions of the surface not completely covered by HA are still visible. After 14 days in SBF, the surface became enriched with HA balls, which in some areas, also appeared agglomerated (Fig 5b). For BG_F, after 7 days in SBF, the micrograph (Fig. 5c) showed the appearance of HA crystallites on the surface of the scaffold while some areas on the surface of the glass-ceramic were not completely covered by HA. On the 14th day in SBF, the HA crystallites appeared to completely cover the sample surface while some pores initially present on the parent glass-ceramic were retained.

The elemental composition of the sample surfaces after the immersion duration in SBF was also monitored for HA nucleation with the aid of EDX spectra and are presented in Fig. 6. After immersion of BG for 7 days, the K peak disappeared and the Si peak declined slightly in intensity (Fig. 6a). At the same time, the peaks for Ca and P appreciated marginally. A further decline in the Si peak was observed after incubation for 14 days (Fig. 6b), while there was a simultaneous slow increase in P as observed in the table inset. These manifestations were in agreement with a material undergoing surface reaction in physiological fluids

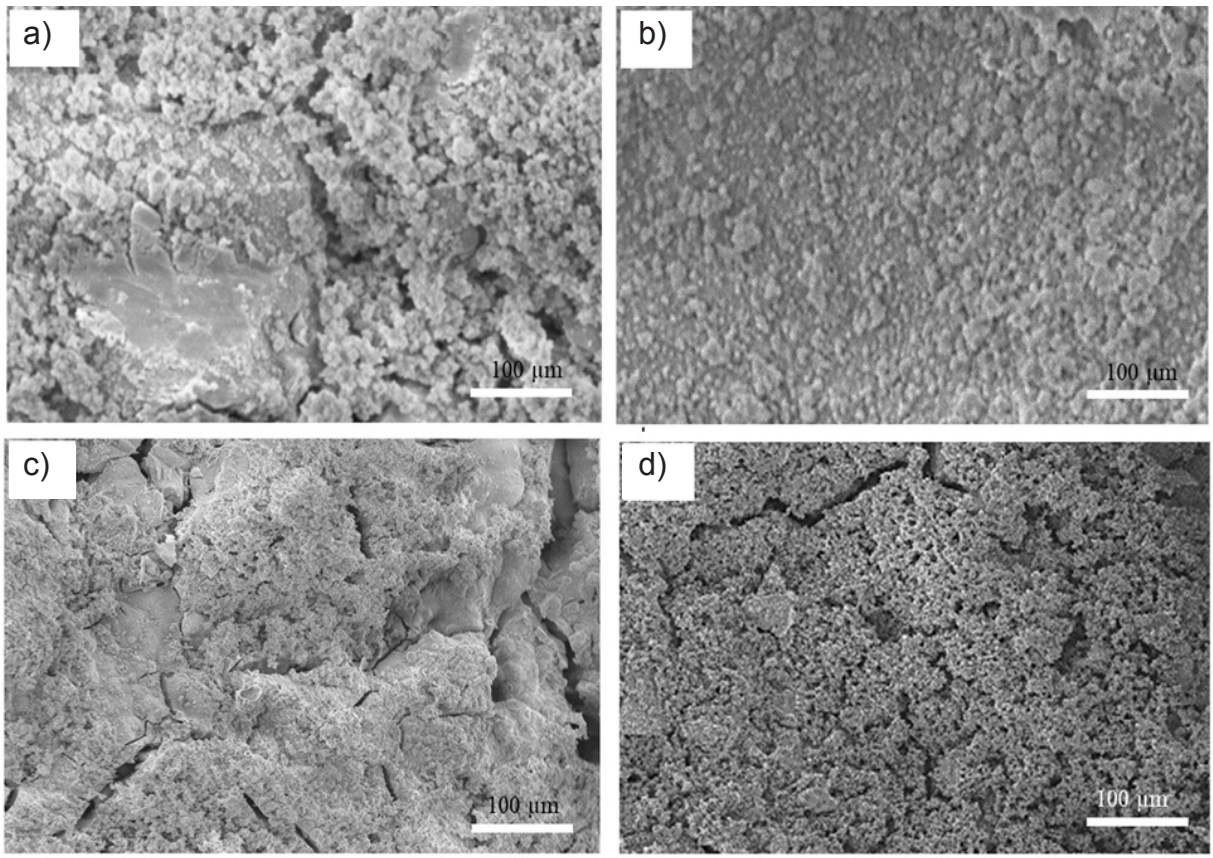

Figure 5: SEM micrographs of BG (a,b) and BG_F (c,d) glass-ceramic samples after immersion in SBF for 7 days (a,c) and 14 days (b,d).

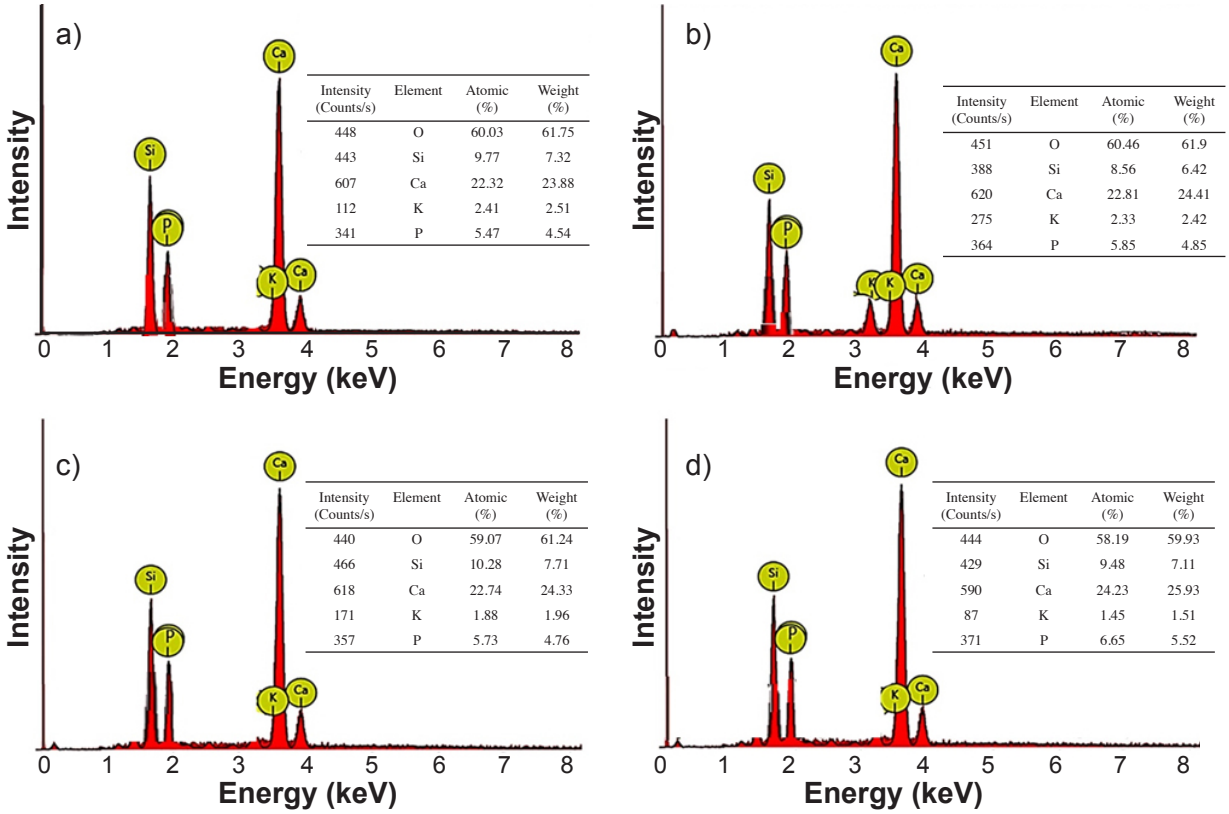

a)

Intensity (Counts/s)	Element	Atomic (%)	Weight (%)
448	O	60.03	61.75
443	Si	9.77	7.32
607	Ca	22.32	23.88
112	K	2.41	2.51
341	P	5.47	4.54

b)

Intensity (Counts/s)	Element	Atomic (%)	Weight (%)
451	O	60.46	61.9
388	Si	8.56	6.42
620	Ca	22.81	24.41
275	K	2.33	2.42
364	P	5.85	4.85

c)

Intensity (Counts/s)	Element	Atomic (%)	Weight (%)
440	O	59.07	61.24
466	Si	10.28	7.71
618	Ca	22.74	24.33
171	K	1.88	1.96
357	P	5.73	4.76

d)

Intensity (Counts/s)	Element	Atomic (%)	Weight (%)
444	O	58.19	59.93
429	Si	9.48	7.11
590	Ca	24.23	25.93
87	K	1.45	1.51
371	P	6.65	5.52

Figure 6: EDX spectra of BG (a,b) and BG_F (c,d) glass-ceramic samples after immersion in SBF for 7 days (a,c) and 14 days (b,d).

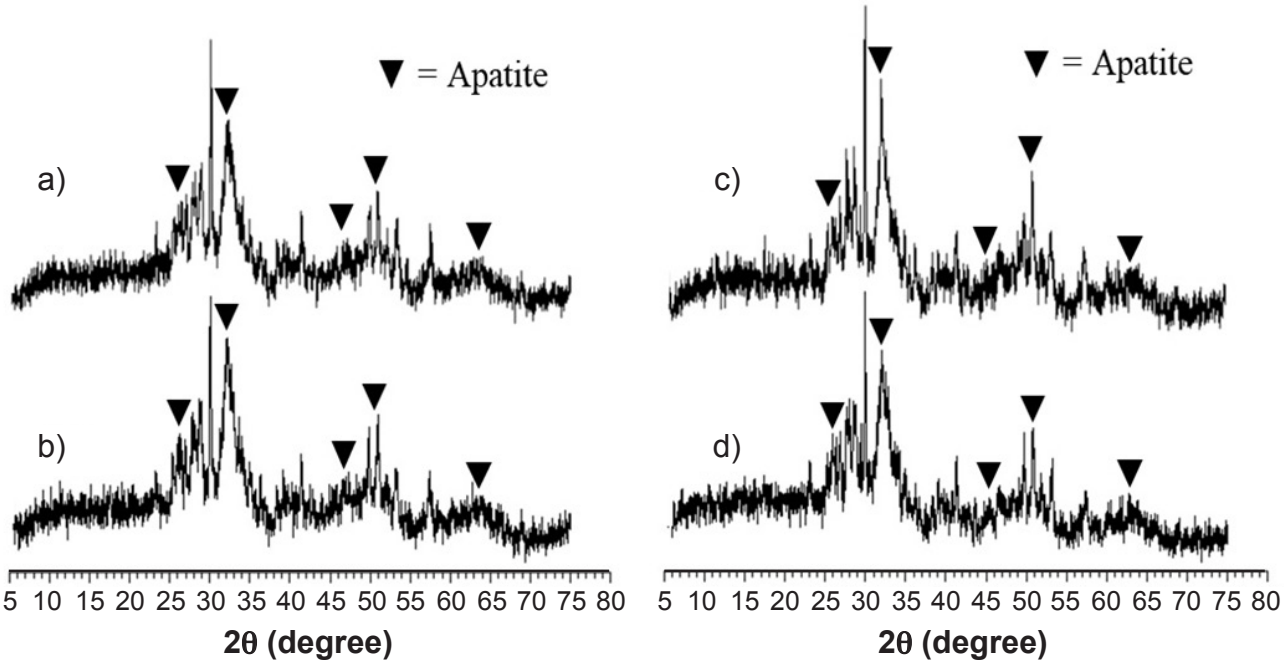

Figure 7: XRD patterns of the glass-ceramic samples after immersion in SBF showing the growth of apatite: a) BG for 7 days; b) BG for 14 days; c) BG_F for 7 days; and d) BG_F for 14 days.

to form HA [12, 32]. During the initial stages in SBF, a glass undergoes a rapid ion-exchange reaction between the glass and the SBF, leading to an exchange of K^+ from the glass and H^+ or H_3O^+ from SBF, consequently, K^+ was depleted from the glass due to its dissolution into the SBF. During the next stages, reabsorption of Ca^{2+} and P from the SBF resulted in an increase in their concentration on the glass surface and hence formed HA [33]. The decrease in Si intensity was attributed to an increase in HA density on the surface of the glass-ceramic as well as degradability in the SBF [10] which led to low detection of Si [18]. A similar reaction was observed for BG_F as was evident in the compositional changes after immersion in SBF for 7 and 14 days, which are depicted in the EDX spectra (Figs. 6c and 6d, respectively).

Further evidence of apatite formation on the samples during the incubation experiment in SBF was provided by the XRD results in Fig. 7. When the peaks were matched in both angular location and intensity [33], HA peaks were identified in BG after soaking for 7 days (Fig. 7a) at 2θ of 25.8°, 32.0°, 46.6°, 51.2°, and 63.8° corresponding to the reflection indices of the hkl plane at 002, 112, 222, 140 and 304, respectively. After immersion for 14 days, the HA peaks increased in intensity (Fig. 7b) indicating an increase in HA density on the surface of the sample, thus supporting the SEM result in Fig. 5. This trend was sustained in BG_F as observed in the diffractograms (Figs. 7c and 7d) which exhibited similar diffraction patterns to BG. It was equally observed that the silicate peaks declined in intensity upon increased immersion duration in SBF compared with the pristine samples (Fig. 3). This may be associated with

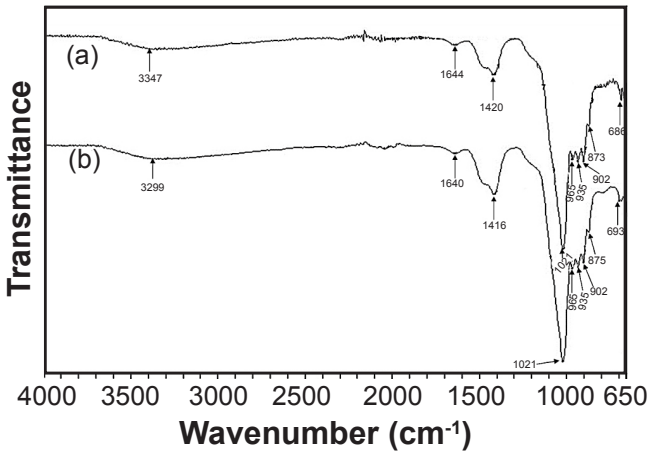

Figure 8: FTIR spectra showing vibrational modes of BG soaked in SBF for 7 days (a) and 14 days (b).

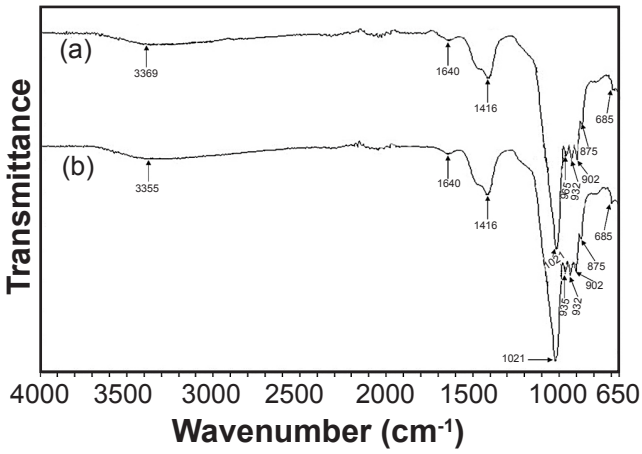

Figure 9: FTIR spectra showing vibrational modes of BG_F soaked in SBF for 7 days (a) and 14 days (b).

the degradation of the silicate peaks as stated earlier. One major concern about glasses in the system SiO_2-Na_2O-CaO-P_2O_5 is that on sintering they crystallize to form combeite ($Na_2Ca_2Si_3O_9$), which adversely affects their degradability in biological fluids [9-14]. It is quite remarkable, therefore, that the samples herein obtained by substituting Na_2O with K_2O in the composition possessed two important attributes: bioactivity and biodegradability. The parent peaks still observed in the spectrum at high intensity after the immersion experiment were mainly those of $CaSiO_3$ and $CaCO_3$. Even though K_2CaSiO_4 presented some degree of crystallinity after sintering, it became resorbable in SBF as evidenced by its low baseline intensity after the incubation experiment. Thus, crystallinity did not jeopardize the bioactivity of K_2CaSiO_4. This was in contrast to crystalline $Na_2Ca_2Si_3O_9$ which decreases the rate of HA formation on a glass surface [11]. The degradation kinetics of a scaffold must match the regeneration kinetics of new bone *in vitro* and/or *in vivo* to have a useful application as an implant [10].

FTIR spectroscopy was used to confirm the presence of bonds related to HA in the samples. For BG, after immersion in SBF for 7 days (Fig. 8a) the vibrational modes showed that the doublet at 1476 and 1405 cm^{-1} fused into a single band centered at 1420 cm^{-1}. At the same time, a shoulder developed at 873 cm^{-1}, suggesting carbonate incorporation to give crystalline HA [34]. Further evidence of the formation of crystalline HA was provided by the emergence of the small peak around 965 cm^{-1} due to the presence of P-O bonds in crystalline HA [35]. The formation of apatite-like crystals was also indicated by the small peak near 686 cm^{-1} in the spectrum resulting from symmetric valence oscillations of the P-O-P bridge bonds, formed by the condensation of the PO_4^{3-} tetrahedron due to better structural ordering [36, 37]. After immersion for 14 days in SBF (Fig. 8b), the vibrational modes of the HA-related bonds did not change significantly, only a slight increase in the intensity of the carbonate band around 1416 cm^{-1} was observed. This was in consonance with the SEM result shown in Fig. 5. A similar trend was observed in the FTIR spectra of BG_F immersed in SBF for 7 and 14 days, as shown in Fig. 9.

CONCLUSIONS

A glass-ceramic scaffold of the SiO_2-K_2O-CaO-P_2O_5 system was designed and synthesized through a modified sol-gel approach that utilized solution precipitation, reagent encapsulation, and foam replication. Na_2O was substituted with K_2O in the composition to prevent crystallization during thermal treatment to $Na_2Ca_2Si_3O_9$, which reduces bioactivity. A homogeneously porous bioactive glass-ceramic scaffold (porosity: 92%; average pore size: 36±6 μm) with well-distributed pores that retained the pore architecture of the polyurethane foam used as a template for the ceramic coating of the glass was obtained. The porous scaffold induced hydroxyapatite (HA) formation on its surface during *in vitro* bioactivity experiments in simulated body fluid (SBF) for 7 and 14 days which further crystallized through carbonate incorporation. An important finding is that the potassium calcium silicate crystalline phase (K_2CaSiO_4) formed in the glass-ceramic did not impede its bioactivity but it was resorbed when immersed in SBF. These behaviors imply that the material could be tailored to achieve the desirable properties of bioactivity and degradability at a much significantly better rate than those composed of $Na_2Ca_2Si_3O_9$ crystals. Equally significant is that the preparation process is cost-effective and facile, i.e., not requiring highly expensive analytical grade reagents, like alkoxysilanes as silica precursors. Hence an economic process for large-scale preparation of porous, bioactive glass-ceramic scaffolds is achievable through the present method.

ACKNOWLEDGEMENT

The authors wish to thank Engr. Nura Adamu of the National Geological Research Laboratory, Nigerian Survey Agency, Kaduna State, Nigeria for the SEM, EDX, XRD, and FTIR spectroscopy analyses of the samples.

REFERENCES

[1] F.J. O'Brien, Mater. Today **14** (2011) 88.
[2] J.R. Jones, A.R. Boccaccini, in "Cellular ceramics: structure, manufacturing, processing and applications", M. Scheffler, P. Colombo (Eds.), Wiley-VCH, Weinheim (2005) 550.
[3] C. Wu, J. Chang, Interface Focus **2** (2012) 292.
[4] M. Łączka, K. Cholewa-Kowalska, A.M. Osyczka, Ceram. Int. **42** (2016) 14313.
[5] L. Hupa, K.H. Karlsson, M. Hupa, H.T. Aro, Eur. J. Glass Sci. Technol. A **51** (2010) 89.
[6] R.J. Jones, Acta Biomater. **9** (2013) 4457.
[7] O. Peitl, E.D. Zanotto, S.C. Serbena, L.L. Hench, Acta Biomater. **8** (2012) 321.
[8] H. Arstila, L. Hupa, K.H. Karlsson, M. Hupa, J. Non-Cryst. Solids **354** (2008) 722.
[9] V.J. Shirtliff, L.L. Hench, J. Mater. Sci. **38** (2003) 4697.
[10] Q.Z. Chen, I.D. Thompson, A.R. Boccaccini, Biomaterials **27** (2006) 2414.
[11] O. Peitl, G.P. LaTorre, L.L. Hench, J. Biomed. Mater. Res. **30** (1996) 509.
[12] D.C. Clupper, J.J. Mecholsky Jr., G.P. LaTorre, D.C. Greenspan, J. Biomed. Mater. Res. **57** (2001) 532.
[13] D.C. Clupper, J.J. Mecholsky Jr., G.P LaTorre, D.C. Greenspan, Biomaterials **23** (2002) 2599.
[14] L.A. Adams, E.R. Essien, A.T. Adesalu, M.L. Julius, J. Sci. Adv. Mater. Devices **2** (2017) 476.
[15] V.J. Shirtliff, L.L. Hench, J. Mater. Sci. **38** (2003) 4697.
[16] V. Cannillo, A. Sola, Ceram. Int. **35** (2009) 3389.
[17] L.D. Silva, F.C. Puosso, V.O. Soares, O. Peitl Filho, S.D.R. Sabino, F.C. Serbena, M.C. Crovace, E.D. Zanotto, Ceram. Int. **47** (2021) 18720.
[18] L.A. Adams, E.R. Essien, E.E. Kaufmann, J. Asian Ceram. Soc. **6** (2018) 132.
[19] D. Bellucci, V. Cannillo, A. Sola, Mater. Lett. **65** (2011) 1825.

[20] T. Kokubo, H. Takadama, Biomaterials **27** (2006) 2907.
[21] S. Limmahakhun, A. Oloyede, K. Sitthiseripratip, Y. Xiao, C. Yan, Addit. Manuf. **15** (2017) 93.
[22] N. Abbasi, S. Hamlet, R.M. Love, N.-T. Nguyen, J. Sci. Adv. Mater. Devices **1** (2020) 5.
[23] Q.L. Loh, C. Choong, Tissue Eng. B **19** (2013) 485.
[24] C.M. Murphy, M.G. Haugh, F.J. O'Brien, Biomaterials **31** (2010) 461.
[25] L. Morejon, J.A. Delgado, A.A. Ribeiro, M.V. de Oliveira, E. Mendizaba, I. Garcia, A. Alfonso, P. Poh, M. van Griensven, E.R. Balmayor, Int. J. Mol. Sci. **20** (2019) 1790.
[26] P. Kongsuwan, G. Brandal, Y.L. Yao, J. Manufac. Sci. Eng. **137** (2015) 31004.
[27] X. Liu, C. Din, P.K. Chu, Biomaterials **25** (2004) 1755.
[28] V. Aina, G. Malavasi, P.A. Fiorio, L. Munaron, C. Morterra, Acta Biomater. **5** (2009) 1211.
[29] B.C. Babu, S. Buddhudu, J. Spectrosc. Dyn. **4** (2014) 5.
[30] R.L. Frost, R. Scholz, A. López, Y. Xi, Spectrochim. Acta A Mol. Biomol. Spectrosc. **124** (2014) 243.
[31] M. Cerruti, C. Morterra, Langmuir **20** (2004) 6382.
[32] L.L. Hench, R.J. Splinter, W.C. Allen, T.K. Greenlee, J. Biomed. Mater. Res. **5** (1971) 117.
[33] M.E. Fleet, X. Liu, P.L. King, Am. Mineral. **89** (2004) 1422.
[34] L.A. Adams, E.R. Essien, J. Adv. Ceram. **5** (2016) 47.
[35] G.D. Sasso, Y. Asscher, I. Angelini, L. Nodari, G. Artioli, Sci. Rep. **8** (2018) 12025.
[36] Y.M. Moustafa, K. El-Egili, J. Non-Cryst. Solids **240** (1998) 144.
[37] Q. Williams, E. Knittle, J. Phys. Chem. Solids **57** (1996) 41.

(Rec. 15/08/2022, Rev. 22/10/2022, 14/11/2022, Ac. 23/11/2022)

(cc) BY-NC